17th World Conference on Earthquake Engineering, 17WCEE
Sendai, Japan - September 13th to 18th 2020

SEISMIC DAMAGE OF SOFT CLAY LAYER DIRECTLY UNDER THE RIVER LEVEE THAT BECOMES PROMINENT BY L2 EARTHQUAKE

T. Noda[(1)], K. Nakai[(2)]

[(1)] *Professor, Nagoya University, noda@nagoya-u.ac.jp*
[(2)] *Associate Professor, Nagoya University, Nakai@civil.nagoya-u.ac.jp*

Abstract

Conventionally, seismic performance verification and design of river levee have been conducted based on the static method to determine whether the amount of settlement due to liquefaction of sandy layer exceeds the external water level or not. In response to the recent damage survey, in addition to liquefaction of foundation ground, damage of levee body itself due to liquefaction is also considered. However, it is still inadequate that earthquake deformation and instability of clayey soil are not taken into account at all. In this paper, a seismic response analysis was performed on the river levee focused on understanding the behavior of soft clay layer. The analysis code employed as the constitutive model in this study was the soil-water coupled finite deformation analysis code ***GEOASIA***, which incorporates SYS Cam-clay model that allows description of the behavior of soils ranging from sand through intermediate soils to clay within the same theoretical framework.

The Section-A where sandy soil is dominant and the Section-B where a thick clay layer is deposited under the sandy soil were considered. In both sections, the surface sand layer has a small *N*-value and a high risk of liquefaction. In addition, the clay layer of the Section-B is in a soft condition with its *N*-value of 0-2. L1 and L2 earthquakes were input to both sections. The L2 earthquake had a larger acceleration and a longer duration than the L1, and includes many long-period components of more than 1.0 sec. When the L1 earthquake was input, surface sandy layer approached to liquefaction during earthquake, so that the shear strain was large in the surface layer in both sections. However, there was almost no deformation around the levee or deep in the ground. On the other hand, the shear strain of the levee and the surface sandy layer became larger in the case of L2 earthquake. That is, the liquefaction enlarged due to the strong shaking. In the case of Section-B, the shear strain increased in the levee and surface sandy layer, which is the same as in Section-A, but in addition to this, a large shear strain was also generated in the soft clay layer directly under the levee. In the case of L1 earthquake, the clay layer was kept stable. However, the clay layer was disturbed by the large shaking of the L2 earthquake. These results suggest the risk of underestimating seismic damage, especially when using the conventional method on the ground where soft clay is dominant.

Keywords: seismic response analysis, river levee, soft clay, soil disturbance, L1&L2 earthquakes

1. Introduction

In the 2011 off the Pacific coast of Tohoku Earthquake, more than 2000 river levees were damaged in a wide area across the jurisdictions of the Tohoku and Kanto Regional Development Bureaus [1]. The degree of damage ranged from minimal cracks to serious damage such as settlement, lateral flow, and slippage in the body of the river levees. According to a survey taken after the earthquake disaster, the liquefaction of foundation ground and river levee bodies was found to be the main cause of large-scale damage. When liquefaction occurs, the height of a river levee is lowered by lateral flow and consolidation settlement. Because floodplains in Japan are densely populated and contain many high-value properties, river levees are important structures that protect people and property from floods and tidal waves. If a river levee is damaged by an earthquake, there is a risk of significant inundation not only from the tsunami that often follows the earthquake, but also from rising water levels associated with tidal waves that may occur before the levee is restored. However, the conventional seismic performance assessment and design focus only on the settlement caused by liquefaction of sandy foundation ground. Moreover, for simplicity, the seismic lateral force is often converted into an equivalent static lateral force. Therefore, conventional seismic design might underestimate and/or overlook seismic damage under other conditions. For instance, after the investigation of the 2011 off the Pacific coast of Tohoku Earthquake, the damage to river levees constructed on clayey foundations has attracted more attention. Moreover, it has been discussed that, in addition to the liquefaction of the foundation, the settlement and deformation of the river levee body caused by liquefaction should be considered to improve the accuracy of damage predictions. Nevertheless, the improved method remains insufficient because it only accounts for the liquefaction damage, and the deformation and destabilization of clayey soil by seismic motion are not considered.

In this paper, seismic response analysis for two different ground motion levels was performed for actual existence river levees located on soft ground. From the comparison of the section where sandy layer is dominant and the section where soft clayey layer is thickly deposited, the effect of soft clayey soil, which was not sufficiently considered in the conventional seismic performance inspection, on earthquake damage is examined. The analysis code employed in this study was the soil-water coupled finite deformation analysis code ***GEOASIA*** [2], which incorporates SYS Cam-clay model [3] that allows description of the behavior of soils ranging from sand through intermediate soils to clay within the same theoretical framework.

2. Geological Composition of Analysis Section

The analysis target is the river levee of the Shijimigawa River flowing in Hekinan City, Aichi Prefecture. Shijimigawa River is a second-class river pouring into Mikawa Bay and originated in the early Edo period when it was excavated to drain the water from Aburagafuchi. The soft soil has been thickly deposited, especially near the estuary, because it was gradually stretched along with the reclamation projects along the coast. Figure 1 shows a liquefaction hazard map of Hekinan City [4]. The liquefaction risk is extremely high in the southern part of Hekinan City, including target area. Figure 2 shows a geological section of the Shijimigawa River. There is sluice gate in the middle part of theShijimigawa River. Therefore, by closing it, it is possible to prevent backflow and run-up damage from the tsunami and storm surge caused by the earthquake. On the other hand, there is no special protection facility other than the river levee downstream from the sluice gate, and if the river levee is severely damaged, there is concern about inundation damage in these areas. Focusing on the geological section, the boundary between alluvial and dilluvial layers sinks toward the downstream, and clay, sand and landfill materials are deposited alternatively above it. The ground is formed in the process of sediment flowing and depositing from the upstream. Therefore, the stratum composition viewed in the longitudinal direction is generally a ground with a deeper basement and a finer-grained layer toward the downstream. In this paper, two cross sections A and B were extracted by focusing on the change of stratum composition in the longitudinal direction.

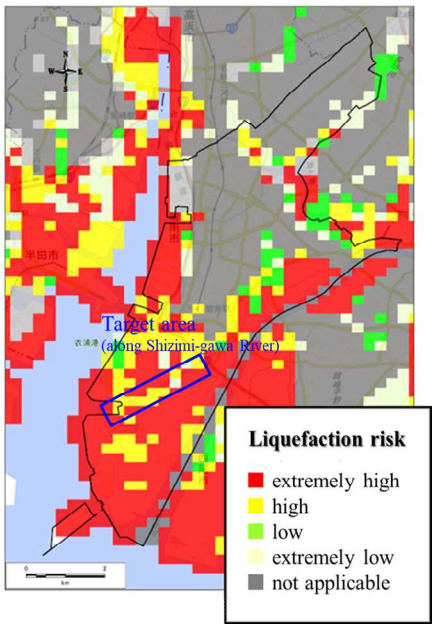

Fig. 1 Liquefaction hazard map

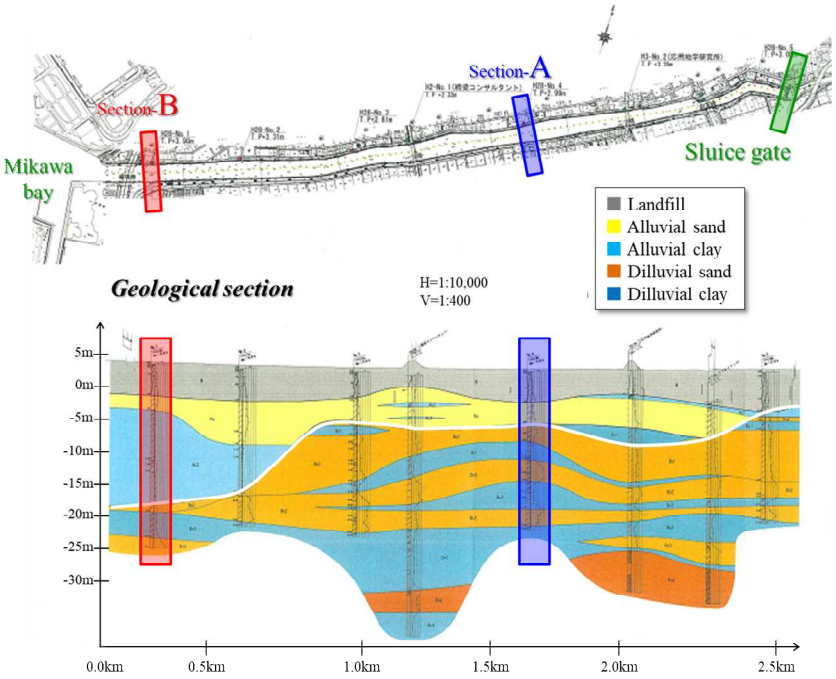

Fig. 2 Geological Section alongShijimigawa River

Section-A is located in the midstream of the Shijimigawa River, where the alluvium is thin and sandy soil is dominant (landfill *B* layer is also sandy material). On the other hand, Section-B is located near the estuary, where the alluvial soft clay is thickly deposited below landfill and alluvial sand. Figures 3 and 4 show the stratum composition diagram at Section-A and Section-B, respectively. The geological composition was estimated from the results of boring surveys performed on both banks of the river. Tables 1 and 2 show physical properties of each layer at both sections. *N*-value indicates the average value for each layer using both boring survey data. In case of Section-A, the basement slopes down gently from the right bank to the left bank. The sedimentary layer is predominantly a sandy layer, and a 3m clayey layer with large *N*-value is deposited in deep. From the physical properties, the alluvial sand layer can be divided into soft layer As_1 and hard layer As_2. *N*-value of subsurface landfill *B* and As_1 are less than 10, and there is a high risk of liquefaction. In case of Section-B, the basement slopes down gently from the left bank to the right bank. Due to the influence of inclination, the clay layer is 20m thick on the right bank and 4m thin on the left bank. Same with Section-A, alluvial sand can be divided into two layers, and subsurface landfill *B* and sand As_1 show high risk of liquefaction because of its low *N*-value. Furthermore, the alluvial clay layer can be divided into two layers. The upper layer Ac_1 has smaller fine particle content than the lower layer Ac_2, and is actually classified as silt. Ac_1 layer has a smaller *N*-value than Ac_2 layer and considered to be in a very soft condition. As a seismic countermeasure, sheet piles are installed on the left bank of both sections. The sheet piles have been installed into diluvium *D* layer.

Table 1 Physical properties of each layer at Section-A

	average *N*-value	fine content	clay content
B	6.9	8.1	5.0
As_1	7.0	14.7	7.0
As_2	25.0	24.8	10.0
Ac_1	10.2	72.6	34.6
D	32.2	14.2	7.0

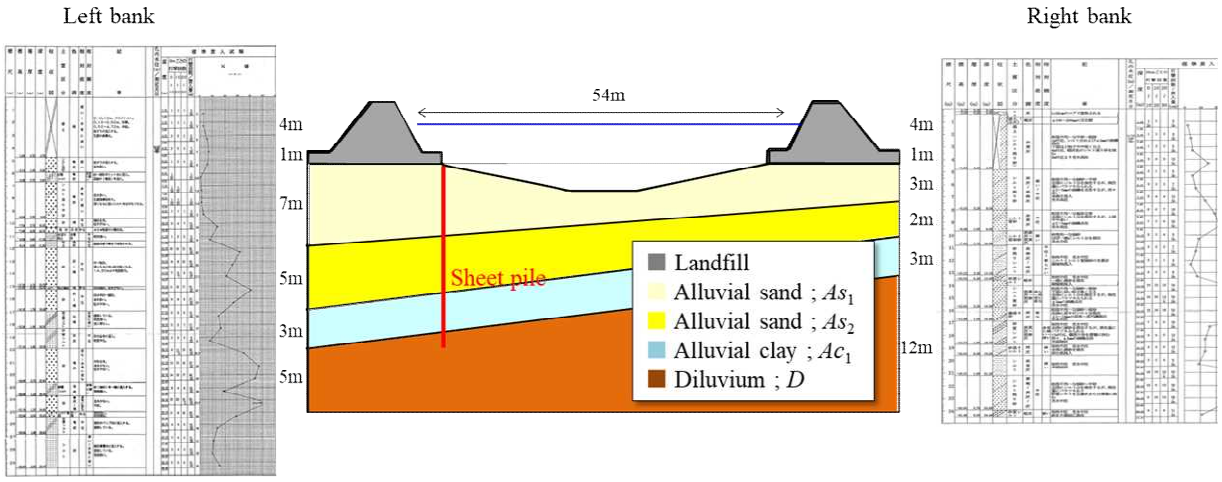

Fig. 3 Stratum composition of Section-A

Table 2 Physical properties of each layer at Section-B

	average *N*-value	fine content	clay content
B	6.0	8.5	5.0
As_1	7.4	7.0	3.0
As_2	27.5	13.0	7.0
Ac_1	1.7	77.0	40.7
Ac_2	3.2	98.3	71.0
D	13.0	92.8	41.3

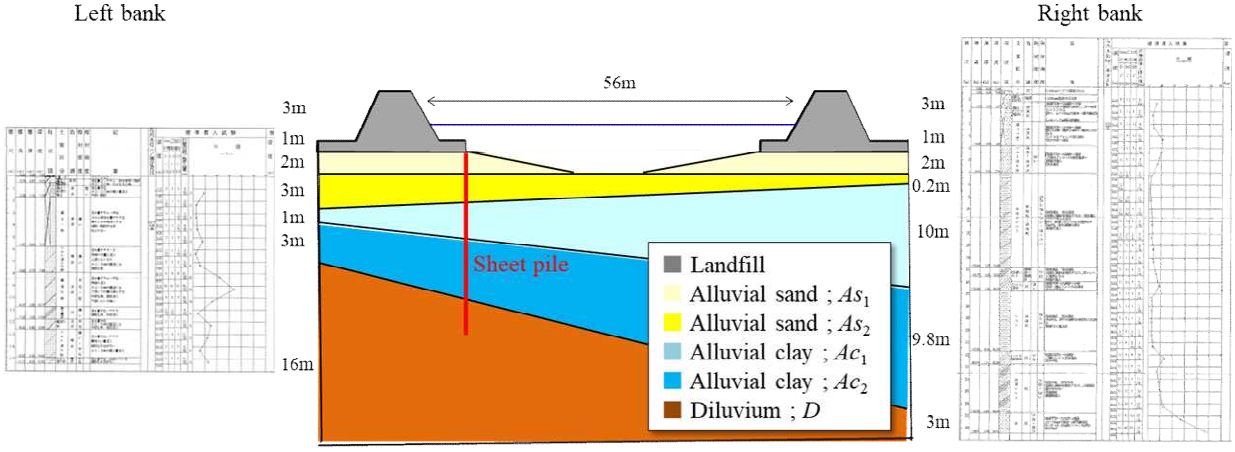

Fig. 4 Stratum composition of Section-B

3. Analytical Conditions

Figures 5 and 6 show the finite element mesh of the target ground respectively. The figure enlarges the central part (around river levee), and the analysis region were originally set as 400 m in width for both sections. The surface of the initial ground was assumed to be horizontal ground. Embankments were constructed on the initial ground by adding finite element meshes [5]. The crown of both levees were 4 m with slope gradients of 1:3. After the levee construction, the river channel was excavated by removing the finite element meshes [5], and the river water level was made to rise up to Tokyo Peil T.P. + 1.2 m. The

hydraulic boundaries for the subsurface were designed as drained boundaries, and the bottom end and the two lateral faces were designed to be under undrained conditions. Although the levee body is usually in an unsaturated condition, the levee was treated as saturated soil to represent the condition most relevant to the problem under investigation, such as after heavy rainfall or inundation by tidal waves. Accordingly, the hydraulic pressure was maintained to be always zero on the surface of the land side of the levees and foundation ground. On the surface of the river side of the levees, the hydraulic pressure was assigned according to the water level height. Periodic boundaries were realized by tying two nodes with the same height between both lateral ends [6, 7].

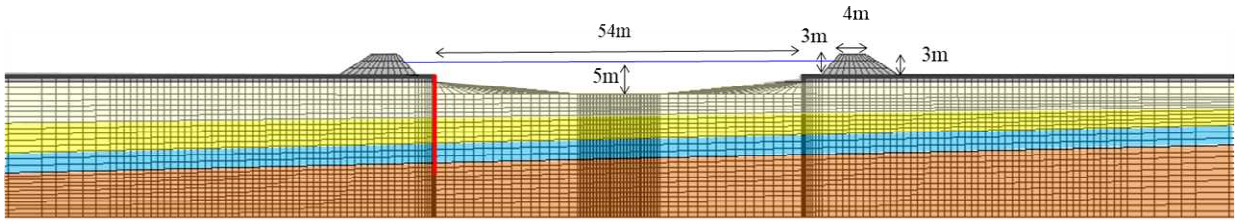

Fig. 5 Finite element mesh for Section-A

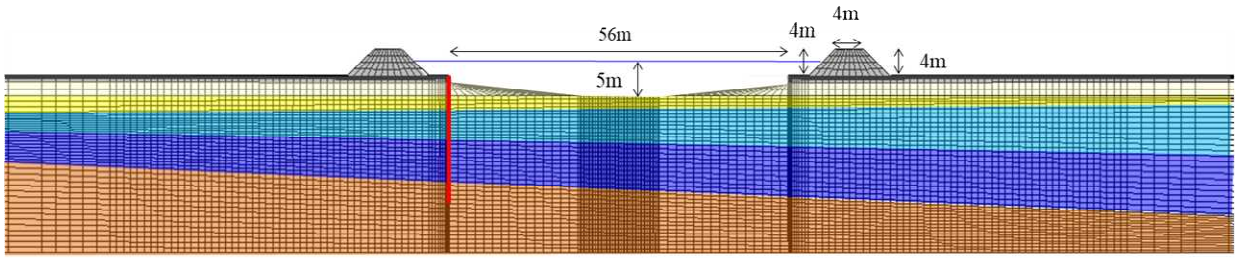

Fig. 6 Finite element mesh for Section-B

The elasto-plastic properties (material constants and initial conditions) of the landfill, alluvial sand, alluvial clay and diluvium layers were all determined based on the results of boring survey conducted at actual site. Tables 3 and 4 list the elasto-plastic properties of each soil layer used in the analysis. In the initial ground conditions, it was presumed that the degree of the soil skeleton structure and the stress ratio were uniform in each layer, and the specific volume was distributed in accordance with the overburden pressure. Sheet pile was modeled as a one-phase linear elastic material. The sheet piles were assumed to be continuously connected perpendicular to the page; however, the analysis was conducted under two-dimensional plane strain conditions. Therefore, the density, Young's modulus was revised so that the weight, flexural rigidity became equivalent to the actual values, as shown in Table 5.

Figures 7 and 8 show two input seismic motions. In this study, two ground motions with different seismic levels were used. "Earthquake motion level 1 (L1 earthquake)" refers to a medium-scale earthquake that is likely to be affected more than once during the use of the structure. "Earthquake motion level 2 (L2 earthquake)" is the strongest earthquake that the structure will receive in the past and in the future, that is, the largest earthquake within a supposed range. L1 earthquake is the assumed ground motion at the nearby Tokoname Port published by the National Institute for Land and Infrastructure Management [8]. L2 earthquake is the assumed ground motion that newly included a long-period component in the Nankai Trough earthquake around the site published by the Cabinet Office [9, 10]. Compared to the L1 earthquake, the L2 earthquake has a large maximum acceleration and a long duration, and contains many long-period components of 1.0 second or more. These seismic motions are defined at the engineering bedrock with its shear wave velocity V_s = 700 m/s. Therefore, the input value was amplified approximately 1.33 times in accordance with the V_s ratio between the engineering bedrock and the bottom end of the analytical region [11,

12]. A viscous boundary [13] equivalent to V_s = 400 m/s was assumed in the horizontal direction on all nodes of the bottom face, and the seismic waveform was input in the horizontal direction equally on all nodes of the bottom face of the ground.

Table 3 Elasto-plastic properties of each soil layer for Section-A

	B	As_1	As_2	Ac_1	*D*
Elasto-plastic parameter					
Compression index λ	0.047	0.047	0.050	0.091	0.047
Swelling index κ	0.0047	0.0047	0.0050	0.0091	0.0047
Critical state index M	1.58	1.58	1.58	1.55	1.58
Intercept of NCL N	1.66	1.66	1.67	1.86	1.66
Poisson's ratio v	0.3	0.3	0.3	0.3	0.3
Evolutional parameter					
Degradation parameter of structure a(b=c=1.0)	1.34	1.34	0.30	0.94	1.34
Degradation parameter of structure c_s	1.0	1.0	1.0	1.0	1.0
Degradation parameter of overconsolidation m	1.28	1.28	1.34	2.65	1.28
Evolution parameter of anisotropy b_r	0.0	0.0	0.0	0.0	0.0
Limit of rotation m_b	1.0	1.0	1.0	1.0	1.0
Initial condition					
Specific volume v_0					
Stress ratio η_0	0.545	0.545	0.545	0.545	0.545
Degree of structure $1/R^*_0$	2.63	2.45	1.81	3.66	2.03
Degree of overconsolidation $1/R_0$	2.63	2.45	1.81	3.66	41.3
Degree of anisotropy ζ_0	0.0	0.0	0.0	0.0	0.0

Table 4 Elasto-plastic properties of each soil layer for Section-B

	B	As_1	As_2	Ac_1	Ac_2	*D*
Elasto-plastic parameter						
Compression index λ	0.047	0.046	0.048	0.15	0.30	0.12
Swelling index κ	0.0047	0.0046	0.0048	0.015	0.03	0.012
Critical state index M	1.58	1.58	1.58	1.52	1.45	1.54
Intercept of NCL N	1.66	1.65	1.66	2.15	2.83	1.99
Poisson's ratio v	0.3	0.3	0.3	0.3	0.3	0.3
Evolutional parameter						
Degradation parameter of structure a(b=c=1.0)	1.34	1.35	1.33	0.57	0.17	0.74
Degradation parameter of structure c_s	1.0	1.0	1.0	0.2	0.2	0.2
Degradation parameter of overconsolidation m	1.28	1.26	1.30	7.44	87.3	4.31
Evolution parameter of anisotropy b_r	0.0	0.0	0.0	0.0	0.0	0.0
Limit of rotation m_b	1.0	1.0	1.0	1.0	1.0	1.0
Initial condition						
Specific volume v_0						
Stress ratio η_0	0.545	0.545	0.545	0.545	0.545	0.545
Degree of structure $1/R^*_0$	2.70	2.53	1.55	4.06	4.04	3.47
Degree of overconsolidation $1/R_0$	23.7	26.9	70.6	2.83	2.87	4.07
Degree of anisotropy ζ_0	0.0	0.0	0.0	0.0	0.0	0.0

Table 5 Material parameters for sheet pile

Young's modulus E (GPa)	30.0
Poisson's ratio v	0.30
Density ρ (g/cm^3)	2.60

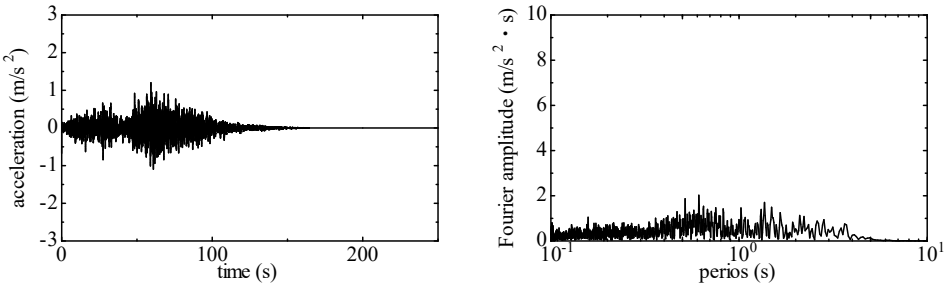

Fig. 7 Seismic motions (L1 earthquake)

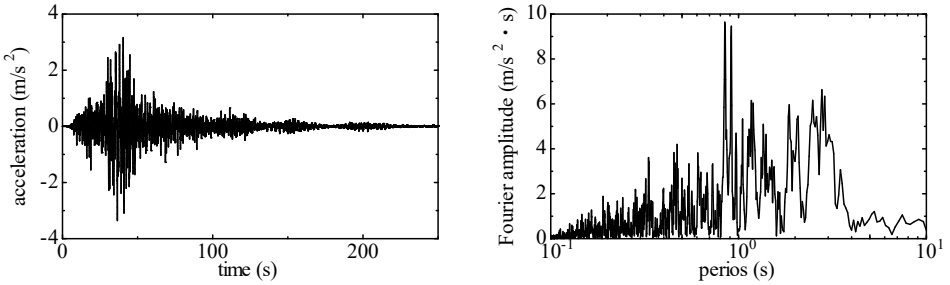

Fig. 8 Seismic motions (L2 earthquake)

4. Analysis Results

4.1 In case of L1 earthquake

Figures 9 and 10 show the mean effective stress and shear strain distributions respectively, 150 seconds after the occurrence of the earthquake (immediately after the earthquake) when the L1 earthquake was input to the Section-A. Mean effective stress of subsurface layer became almost zero, which indicates the occurrence of liquefaction. However, since the liquefaction was limited to the subsurface layer, shear strain was small, and it was generated only in the levee and directly below it. Figures 11 and 12 show the amount of settlement at the levee crown and lateral displacement at the foot of levee slope respectively. Lateral displacement at the bottom of the levee hardly occurred on both banks. The crown height was reduced by 0.5m on the left bank and 0.6m on the right bank. Most of this settlement occurred on levee itself. In this analysis, the levee was modeled as a saturated soil, so the deformation at the levee is considered to be larger than in the normal unsaturated condition. However, the height of the river levee after the earthquake did not exceed the assumed limit water level, and the river levee is considered to maintain its function during the L1 earthquake.

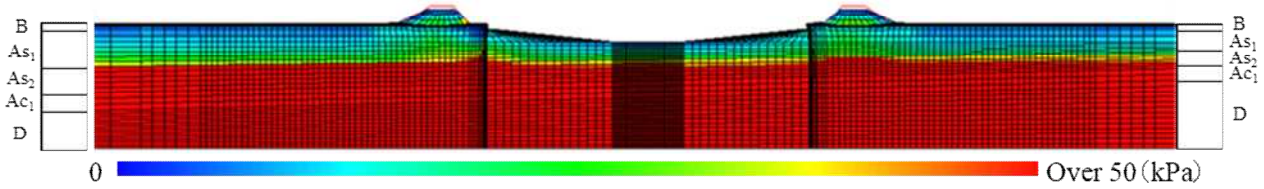

Fig. 9 Mean effective stress distribution (L1 earthquake, Section-A)

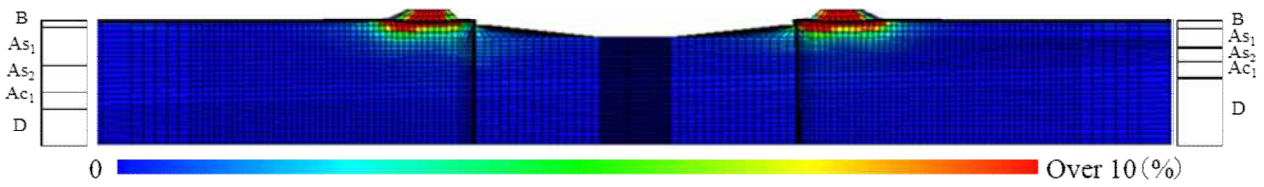

Fig. 10 Shear strain distribution (L1 earthquake, Section-A)

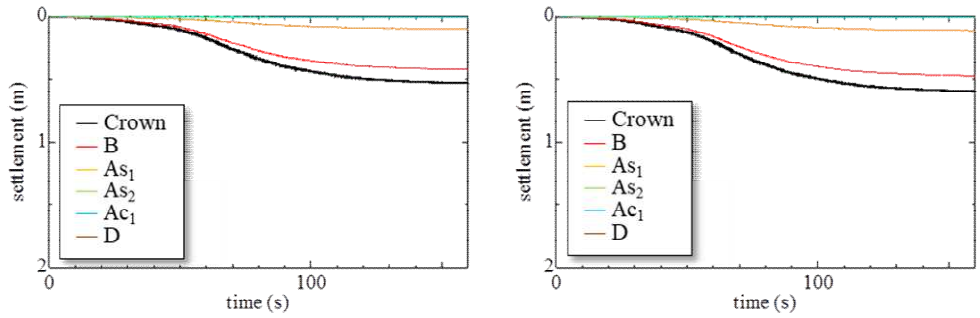

(a) Left bank embankment crown (b) Right bank embankment crown

Fig. 11 Settlement at the levee crown (L1 earthquake, Section-A)

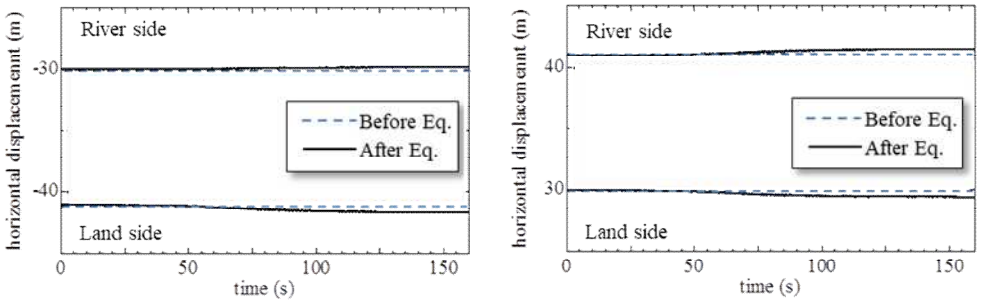

(a) Left bank embankment foot of slope (b) Right bank embankment foot of slope

Fig. 12 Lateral displacement at the bottom toe of levee (L1 earthquake, Section-A)

Figures 13 and 14 show the mean effective stress and shear strain distributions respectively, 150 seconds after the occurrence of the earthquake when the L1 earthquake was input to the Section-B. As in Section-A, mean effective stress was reduced at the subsurface layer which indicating liquefaction, and shear strain was generated under the levee and directly below the levee. Shear strain was also generated in the soft clay Ac_1 layer to some extent directly below the levee, but it did not affect much to the deformation of the levee. Figures 15 and 16 show amount of settlement at the levee crown and lateral displacement at the foot of levee slope respectively. Lateral displacement at the bottom of the levee hardly occurred on both banks. The crown height was reduced by 0.5m on the left bank and 0.6m on the right bank. As in Section-A, river levee is considered to keep its function during the L1 earthquake. As shown in the introduction part, the analysis target area is soft ground, and the risk of liquefaction is originally high. Therefore, even in the case of L1 earthquake, liquefaction easily occurred in both sections at the subsurface sandy soil layer. However, because the degree of liquefaction was small, seismic damage due to the earthquake was very small and levee could maintain its anti-seismic function.

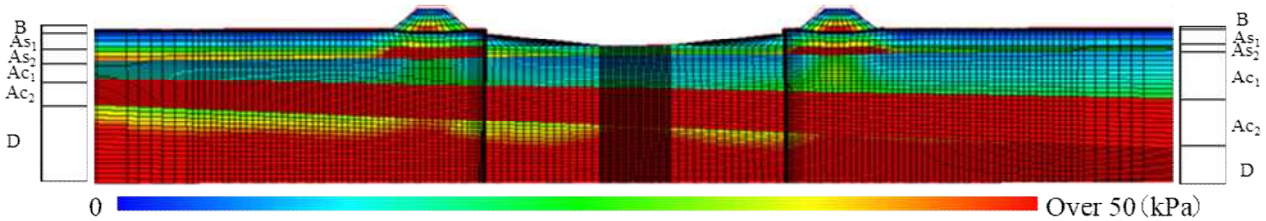

Fig. 13 Mean effective stress distribution (L1 earthquake, Section-B)

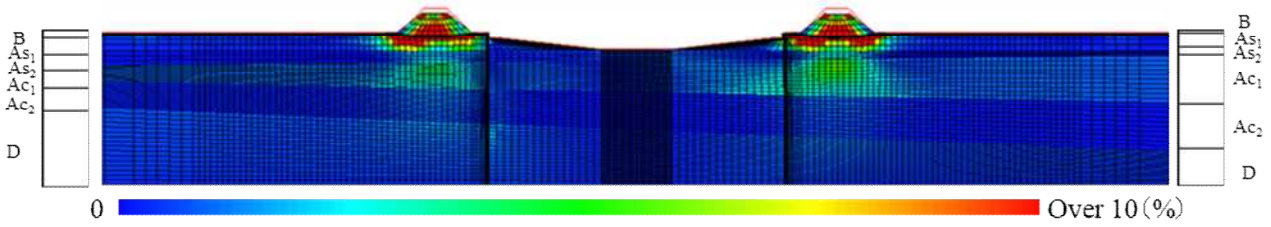

Fig. 14 Shear strain distribution (L1 earthquake, Section-B)

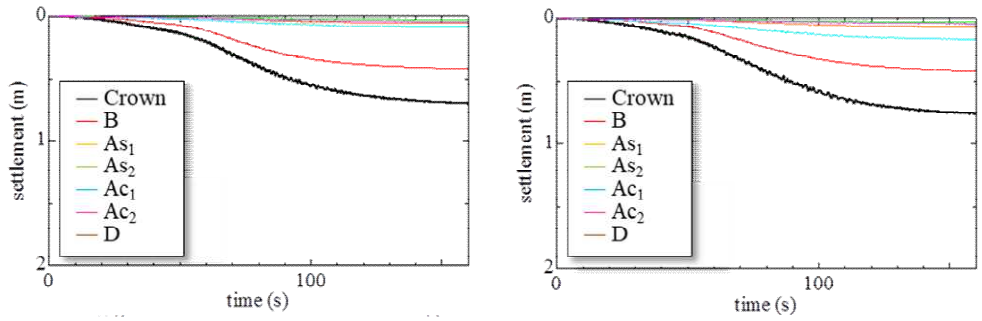

(a) Left bank embankment crown (b) Right bank embankment crown

Fig. 15 Settlement at the levee crown (L1 earthquake, Section-B)

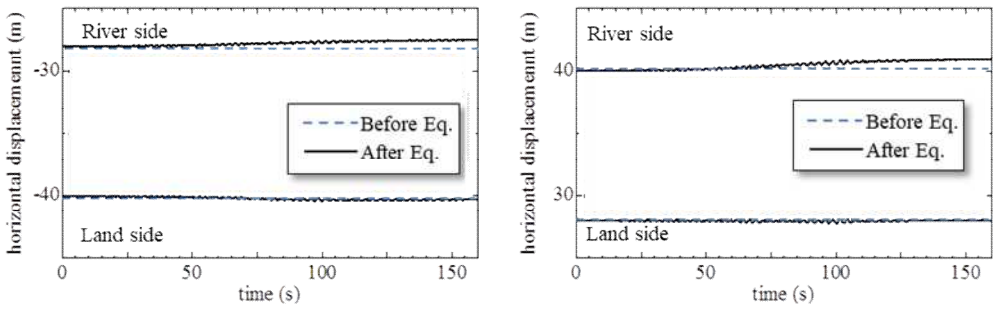

(a) Left bank embankment foot of slope (b) Right bank embankment foot of slope

Fig. 16 Lateral displacement at the bottom toe of levee (L1 earthquake, Section-B)

4.2 In case of L2 earthquake

Figures 17 and 18 show the mean effective stress shear strain distributions respectively, 250 seconds after the occurrence of the earthquake (immediately after the earthquake) when the L2 earthquake was input to the Section-A. Compared to the L1 earthquake, mean effective stress reduction of the landfill *B* layer and alluvial sand As_1 layer is larger, and liquefaction becomes severer. Along with that, the shear strain under the levee itself and directly below the levee increased compared to the L1 earthquake. Figures 19 and 20 show amount of settlement at the levee crown and lateral displacement at the foot of levee slope respectively. Unlike the L1 earthquake, lateral displacement occurred at the bottom of the levee on both right and left banks. On the right bank with no sheet pile, it spread to both the river and land side, but on the left bank where the sheet pile is installed, it spread only to the land side of the river. While the lateral displacement to the river side is suppressed by the countermeasures, there is a risk that the lateral displacement on the land side may increase. The crown height was reduced by 1.2m on the left bank and 1.1m on the right bank. In addition to the levee itself, the amount of settlement in As_1 layer increased. This is because the liquefaction of the subsurface sandy layer became enormous due to the long-period and long-continuous shaking by the L2 earthquake.

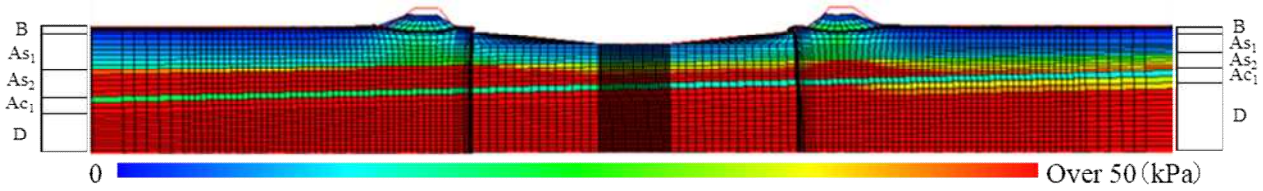

Fig. 17 Mean effective stress distribution (L2 earthquake, Section-A)

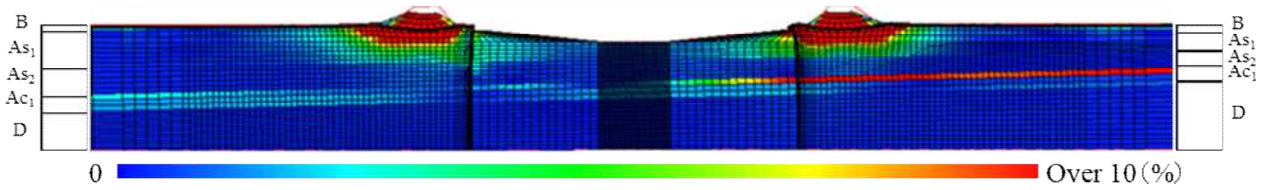

Fig. 18 Shear strain distribution (L2 earthquake, Section-A)

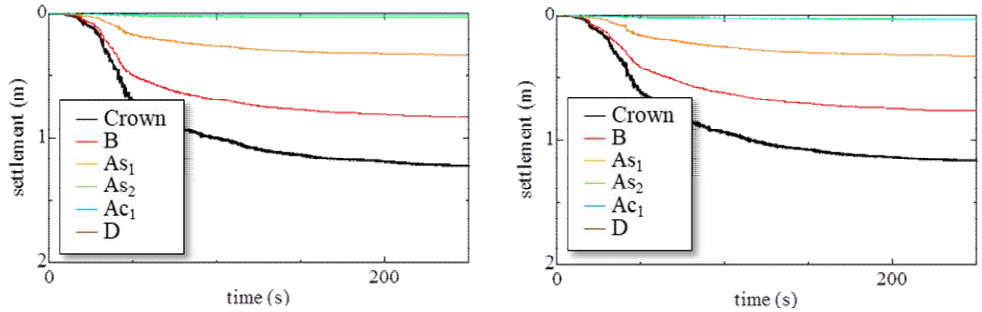

(a) Left bank embankment crown (b) Right bank embankment crown

Fig. 19 Settlement at the levee crown (L2 earthquake, Section-A)

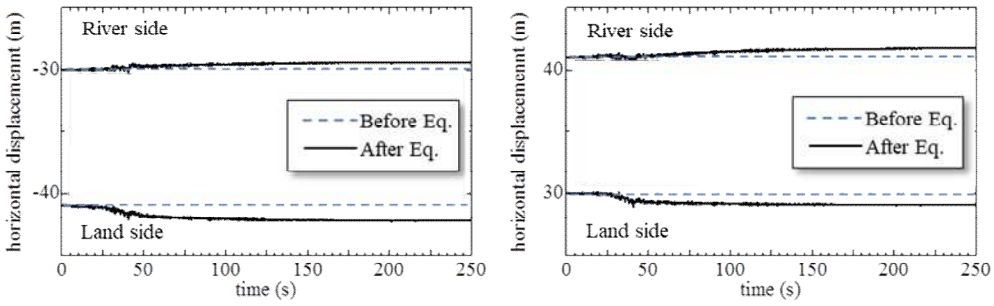

(a) Left bank embankment foot of slope (b) Right bank embankment foot of slope

Fig. 20 Lateral displacement at the bottom toe of levee (L2 earthquake, Section-A)

Figures 21 and 22 show the mean effective stress and shear strain distributions respectively, 250 seconds after the occurrence of the earthquake when the L2 earthquake was input to the Section-B. Mean effective stress was greatly reduced not only in the subsurface sandy layer but also in the upper clay layer Ac_1. As a result, a large shear strain was generated in the Ac_1 layer directly below the levee, which had not been damaged by the L1 earthquake. It can be seen that even in the case of clayey soil, in places where soft and uneven loads are applied, if the strong shaking continues for a long time, the ground may be disturbed and severe seismic damage may occur. Figures 23 and 24 show the amount of settlement at the levee crown and lateral displacement at the foot of levee slope respectively. The crown height was reduced 1.7m on the left bank and 1.9m on the right bank. Liquefaction was exacerbated, and seismic damage was also caused on

clayey layer. Focus on the amount of settlement, it can be seen that the not only in the levee but also Ac_1 became obvious. Therefore, the deformation of the levee (settlement, lateral displacement) became large.

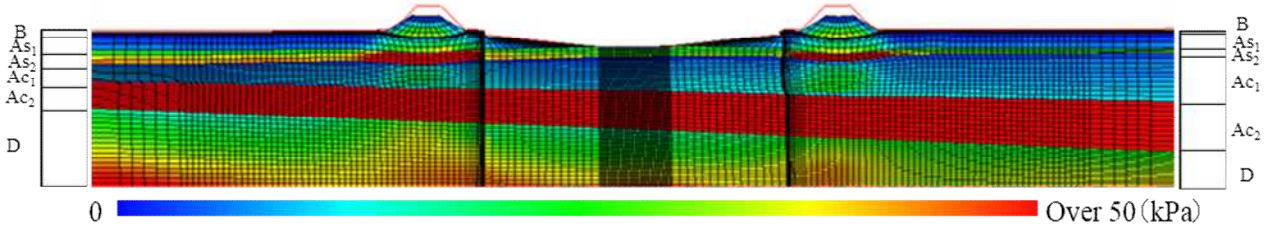

Fig. 21 Mean effective stress distribution (L2 earthquake, Section-B)

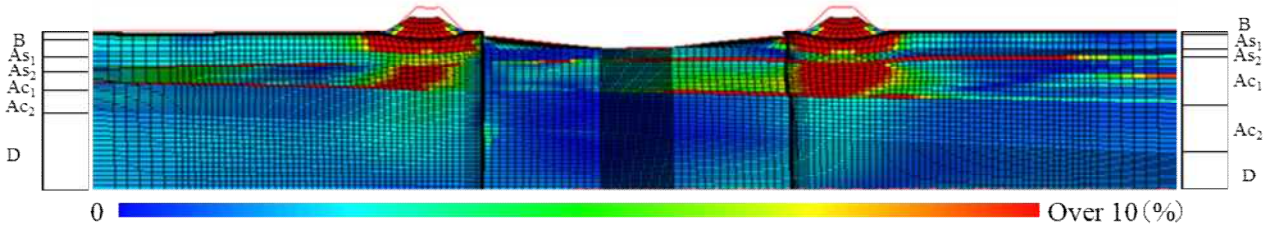

Fig. 22 Shear strain distribution (L2 earthquake, Section-B)

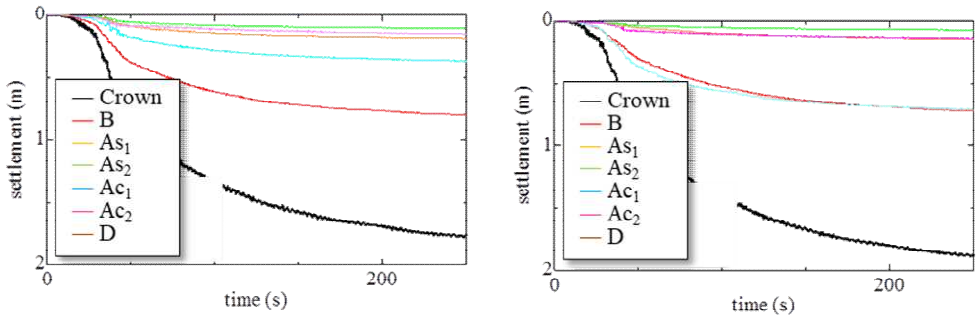

(a) Left bank embankment crown (b) Right bank embankment crown

Fig. 23 Settlement at the levee crown (L2 earthquake, Section-B)

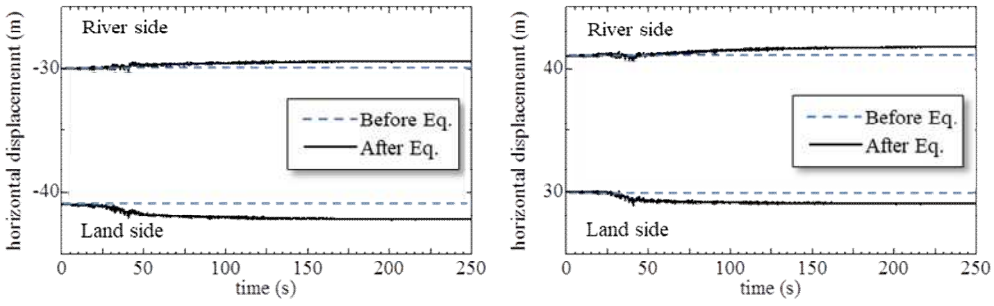

(a) Left bank embankment foot of slope (b) Right bank embankment foot of slope

Fig. 24 Lateral displacement at the bottom toe of levee (L2 earthquake, Section-B)

5. Conclusions and Discussions

Based on the results of the field survey, an elasto-plastic model of the two cross-sections of the Shijimigawa River was prepared to predict ground deformation during L1 and L2 earthquakes. In case of L1 earthquake, the subsurface sandy soil shows liquefaction, but the amount of settlement of the levee was small as less than 20% of the initial height in both sections, and was stable during the earthquake. On the other hand, in case of

L2 earthquake, the settlement of the levee was about 36 to 50%, which was larger than that of L1 earthquake. In addition to the large maximum acceleration, the long duration and long-period components, soft clayey layer directly below the levee under uneven load was strongly disturbed, causing large deformation.

Since the Niigata Earthquake (1964) and the Alaska Earthquake (1964) attracted attention on the liquefaction damage of sandy ground, it has been said that clayey foundation will not be affected by earthquake damage. Therefore, in the conventional seismic damage predictions, even in the case of soft clayey soil, or soil containing much sand and silt, soil that is classified as clayey soil is considered to preclude the possibility of seismic damage, and therefore clayey soil has been always modelled as an elastic material. However, this analysis results indicate that even in the case of clayey soil, in places where soft and uneven loads are applied; like directly below the levee, if the strong shaking continues for a long time, the ground may be disturbed and severe seismic damage may occur. This suggests that there is a risk of underestimating the ground deformation if using the conventional seismic damage prediction method, especially in the case where the soft clay layer is thickly deposited.

6. Acknowledgements

This study was supported by the project “Research project for compound disaster mitigation on the great earthquakes and tsunamis around the Nankai trough region” of the Ministry of Education, Culture, Sports, Science and Technology Japan. We are grateful to the Hekinan City for providing site investigation data.

7. References

[1] Kazama, M., and Noda, T. (2012): Damage statistics: summary of the 2011 off the Pacific Coast of Tohoku Earthquake damage, *Soils and Foundations*, **52**, 5, 780–792.

[2] Noda, T., Asaoka, A. and Nakano, M. (2008): Soil-water coupled finite deformation analysis based on a rate-type equation of motion incorporating the SYS Cam-clay model, *Soils and Foundations*, **48**, 6, 771-790.

[3] Asaoka, A., Noda, T., Yamada, E., Kaneda, K. and Nakano, M. (2002): An elasto-plastic description of two distinct volume change mechanisms of soils, *Soils and Foundations*, **42**, 5, 47-57.

[4] Hekinan City, http://www.city.hekinan.lg.jp/soshiki/shiminkyoudou/bosai/6/1067.html

[5] Takaine, T., Tashiro, M., Shiina, T., Noda, T., and Asaoka, A. (2010): Predictive simulation of deformation and failure of peat-calcareous soil layered ground due to multistage test embankment loading, *Soils and Foundations*, **50**, 2, 245–260.

[6] Asaoka, A., Noda T., and Kaneda, K. (1998): Displacement/traction boundary conditions represented by constraint conditions on velocity field of soil, *Soils and Foundations*, **38**, 7, 173–181.

[7] Noda, T., Takeuchi, H., Nakai, K., and Asaoka, A. (2009): Co-seismic and post-seismic behavior of an alternately layered sand-clay ground and embankment system accompanied by soil disturbance, *Soils and Foundations*, **49**, 5, 739–756.

[8] National Institute for Land and Infrastructure Management, http://www.ysk.nilim.go.jp/kakubu/kouwan/sisetu/sisetu.html

[9] Fukui, Y., Kurata, K., Hirai, K. and Fukuwa, N. (2017): Construction of an earthquake response experience environment of a skyscraper combining virtual reality technology and shaking table, *Annual meeting of Architecture Institute of Japan 2017*, 407-408, in Japanese.

[10] Cabinet Office, Government of Japan, http://www.bousai.go.jp/jishin/nankai/model/

[11] Midorikawa, S. (1987): Prediction of isoseismal map in the Kanto plain due to hypothetical earthquake, *Journal of Structural Engineering*, **33**, B, 43–48, in Japanese.

[12] Sugito, M., Furumoto, Y., and Sugiyama, T. (2000): Strong motion prediction on rock surface by superposed evolutionary spectra, *Proceedings of the12th WCEE*, Paper No. 2111(CD-Rom).

[13] Lysmer, J., and Kuhlemeyer, R.L. (1969): Finite dynamic model for inifinite media, *Journal of the Engineering Mechanics Division*, **98**, EM4, 859–877.

